Entanglement in noncritical inhomogeneous quantum chains

Nadir Samos Sáenz de Buruaga,[1] Silvia N. Santalla,[2] Javier Rodríguez-Laguna,[3] and Germán Sierra[1]
[1]*Instituto de Física Teórica UAM/CSIC, Universidad Autónoma de Madrid, Cantoblanco, 28049 Madrid, Spain*
[2]*Departamento de Física & GISC, Universidad Carlos III de Madrid, 28911 Leganés, Madrid, Spain*
[3]*Departamento de Física Fundamental, Universidad Nacional de Educación a Distancia (UNED), 28040 Madrid, Spain*

(Received 31 July 2021; revised 8 October 2021; accepted 11 November 2021; published 24 November 2021)

We study an inhomogeneous critical Ising chain in a transverse field whose couplings decay exponentially from the center. In the strong inhomogeneity limit, we apply Fisher's renormalization group to show that the ground state is formed by concentric singlets similar to those of the rainbow state of the XX model. In the weak inhomogeneity limit, we map the model to a massless Majorana fermion living in a hyperbolic space-time, where, using conformal field theory techniques, we derive the entanglement entropy and show that it presents a linear scaling. We also study an inhomogeneous noncritical Ising model that for weak inhomogeneity is mapped to a massive Majorana fermion, while for strong inhomogeneity regime, it exhibits trivial and nontrivial topological phases and a separation between regions with high and low entanglement. We also present the entanglement Hamiltonian of the model.

DOI: 10.1103/PhysRevB.104.195147

I. INTRODUCTION

The study of entanglement in quantum many-body systems [1–4] has proven to be an excellent way to advance in the understanding of quantum matter [5]. Given a pure state $|\Psi\rangle$ of a system and a bipartition into two subsystems, $A \cup B$, all the information concerning quantum correlations between these parts is contained in the reduced density matrix $\rho_A = \mathrm{Tr}_B |\Psi\rangle \langle\Psi|$. The most important measure of entanglement is the von Neumann entropy, $S_A = -\mathrm{Tr}\rho_A \ln \rho_A$, that vanishes if and only if the subsystems are disentangled. The low energy states of local quantum Hamiltonians are expected to satisfy the so-called area law, which asserts that the entanglement entropy (EE) of a block is bounded by the size of its boundary [6–9]. This property holds for one dimensional gapped Hamiltonians under certain assumptions [7], but is violated in critical Hamiltonians described by a conformal field theory (CFT), where the EE grows logarithmically with the subsystem size and is proportional to the central charge [10–13].

The study of entanglement in spatially inhomogeneous systems has attracted recently considerable interest. For example, the EE of local Hamiltonians with random couplings exhibits a logarithmic behavior, presenting some similarity with the CFT result [14–19]. Other interesting cases include the engineered trapping potentials for ultracold atoms which reduce the boundary effects [20–23], the interplay between quantum gravity and strange metals within the Sachdev-Ye-Kitaev (SYK) model [24,25], the quantum simulation of the Dirac vacuum on a curved space-time using optical lattices [26–28], or the connection between inhomogeneous XX spin chains and certain quasi-solvable models on the line [29]. In some cases, it is possible to obtain the ground state (GS) of these systems using renormalization group (RG) schemes such as the Dasgupta-Ma procedure [30]. Conversely, the RG can help us design certain lattice models, such as the *rainbow state* (RS), which is the GS of an XX spin-chain whose couplings decay exponentially from the center towards the edges, and which presents a linearly growing EE between its two halves [31–42]. The system is described in terms of an inhomogeneity parameter h, associated to the exponential decay. In the strong inhomogeneity regime, the GS is a nested set of Bell pairs, which can also be described as a concentric singlet state [31,33]. In the weak inhomogeneity regime the rainbow chain corresponds to a free Dirac theory on a (1+1)D anti-de-Sitter space-time [36,38]. Thus the EE can be obtained as a deformation of well-known results from CFT, showing that the logarithmic growth maps into a linear one. Moreover, there is a smooth crossover between the weak and strong inhomogeneity regimes.

In addition to the EE, bipartite entanglement can be characterized by other magnitudes. The density matrix ρ_A can be written as

$$\rho_A \propto e^{-\mathcal{H}_A}, \tag{1}$$

where $\mathcal{H}_A$ is called the entanglement Hamiltonian (EH) associated to a block A within a quantum state [43–49]. Even if the original state is translationally invariant, the EH usually represents an inhomogeneous system, and it has been characterized for several interesting systems, employing e.g. the corner transfer matrix formalism (CTM) [46,49] or CFT results [47]. Moreover, the EH of certain inhomogeneous systems has been described using the RS as a benchmark, showing that it can be understood as a *thermofield double*: each half of the system can be approximated by a homogeneous system at a finite temperature that depends on the inhomogeneity level h [37]. The spectrum of the EH is called the entanglement spectrum (ES), which can provide interesting information e.g. regarding

the existence of symmetry-protected topological phases (SPT) [50–55].

The aim of the present work is twofold. First, to characterize the emergence of a rainbow state as a ground state of an inhomogeneous transverse field Ising (inhomogeneous ITF) Hamiltonian, when the couplings and the external fields are allowed to decay in a certain way, by mapping it to a (1+1)D massless Majorana field on curved space-time. Then, we will describe the structure of the model away from the critical point, showing that it reduces to a massive Majorana field in the same setup. Moreover, we shall also consider the relation between our model and the Kitaev chain [50].

This article is organized as follows. In Sec. II, we introduce an inhomogeneous version of the ITF model and describe its entanglement structure. The strong inhomogeneity regime is discussed by means of RG schemes, and the weak inhomogeneity regime is characterized via field theory methods. In Sec. III, we propose a variation of the previous model by adding a new parameter that shifts it away from the critical point, and we describe its entanglement properties in the strong and weak inhomogeneity regimes. Finally, we present a brief discussion of our conclusions and prospects in Sec. IV.

II. THE ISING RAINBOW STATE

Let us consider an inhomogeneous ITF open spin 1/2 chain with an even number of sites $N = 2L$ whose Hamiltonian is defined as

$$H_I = -\sum_{m=-L+1/2}^{L-3/2} J_m \sigma_m^z \sigma_{m+1}^z - \sum_{m=-L+1/2}^{L-1/2} \Gamma_m \sigma_m^x, \qquad (2)$$

where σ^x and σ^z are Pauli matrices. Notice that the spins are indexed by half-odd integers for later convenience, $m = -L + 1/2, \ldots, L - 1/2$. We shall apply a Jordan-Wigner transformation and write Eq. (2) in terms of Dirac fermions $c_m^\dagger$ which satisfy the usual anticommutation relations $\{c_m^\dagger, c_n\} = \delta_{mn}$, and then decompose them in terms of Majorana fermions

$$c_m = \tfrac{1}{2}(\alpha_m + i\beta_m), \qquad (3)$$

that satisfy the anticommutation relations $\{\alpha_m, \alpha_n\} = \{\beta_m, \beta_n\} = 2\delta_{mn}$ and $\{\alpha_m, \beta_n\} = 0$. In terms of these Majorana fermions, Eq. (2) reads

$$H = -i\left(\sum_{m=1/2}^{L-1/2} \Gamma_m(\alpha_m\beta_m + \alpha_{-m}\beta_{-m}) + \sum_{m=1/2}^{L-3/2} J_m(\beta_m\alpha_{m+1} + \beta_{-(m+1)}\alpha_{-m}) + J_{-1/2}\beta_{-1/2}\alpha_{1/2}\right), \qquad (4)$$

Notice that the same system is described by $2L$ spins and $4N$ Majorana fermions. In Fig. 1, we present a schematic representation of the model in terms of spins (top) and Majorana fermions (bottom). The transverse field Γ_m couples two Majorana fermions with the same index (α_m, β_m), while the coupling constants J_m link Majorana fermions with different indices (β_m, α_{m+1}). The dashed lines that encircle the Majorana fermions represent the Dirac fermions c_m in Eq. (3).

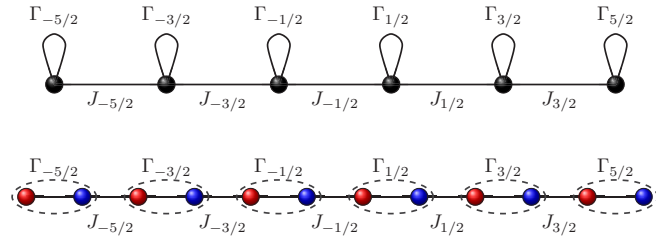

FIG. 1. Spin (top) and Majorana fermion (bottom) representations of the inhomogeneous ITF model. The red (blue) points correspond to α (β) Majorana fermions.

Notice that if $J_m = \Gamma_m = 1$ for all m we recover the critical ITF model whose low-energy behavior is described by the two dimensional Ising CFT with central charge $c = 1/2$. In addition, if $J_m = 0$ for all m, the ground state becomes a trivial product state built upon the physical fermions c_m. On the contrary, if $\Gamma_m = 0$ for all m, the Majorana fermions placed at the edges of the Majorana chain, $\alpha_{-L+1/2}$ and $\beta_{L-1/2}$, do not appear in the Hamiltonian, Eq. (4). Moreover, they correspond to Majorana zero modes and the GS belongs to the topologically nontrivial phase of the Kitaev model [50].

Let us consider both the spin and the Majorana fermion Hamiltonians, Eqs. (2) and (4), under the following choice of coupling constants J_m and Γ_m:

$$J_m = \begin{cases} e^{-2h|m+1/2|} & \text{if } m \neq -1/2, \\ e^{-h/2} & m = -1/2, \end{cases}$$
$$\Gamma_m = e^{-2h|m|}, \qquad (5)$$

where $h \geqslant 0$ is the inhomogeneity parameter. Notice that for $h > 0$, the intensity of the couplings decreases from the center towards the edges, with $J_{-1/2}$ corresponding to the strongest coupling. Also, the system is symmetric under reflections around the central bond, satisfying $J_{-(m+1)} = J_m$ and $\Gamma_m = \Gamma_{-m}$. In the remainder of this section, we shall describe the strong ($h \gg 1$) and weak ($h \ll 1$) inhomogeneity regimes.

A. Strong inhomogeneity

In the limit $h \gg 1$, we can characterize the GS of (4) using the strong disorder renormalization scheme (SDRG) developed by Fisher for the ITF [56,57]. It was devised for finding the ground states of random ITF chains but it can be applied to other kinds of inhomogeneous systems, since the key to the success of the SDRG is not disorder, but inhomogeneity [32,34,35]. Fisher's RG proceeds by finding the strongest interaction coupling, either Γ or J, which gets sequentially decimated. If it corresponds to a magnetic field, Γ_i, the ith spin is integrated out, leaving the system with one spin less and a new coupling term between the spins $i-1$ and $i+1$,

$$\tilde{J}_{i-1}\sigma_{i-1}^z\sigma_{i+1}^z, \qquad \text{with} \quad \tilde{J}_{i-1} = \frac{J_{i-1}J_i}{\Gamma_i}. \qquad (6)$$

On the other hand, if the coupling J_i is the strongest interaction at a given RG step, the spins i and $i+1$ get renormalized into a single spin with effective Hamiltonian

$$\tilde{\Gamma}_i\sigma_i^x, \qquad \text{with } \tilde{\Gamma}_i = \frac{\Gamma_i\Gamma_{i+1}}{J_i}. \qquad (7)$$

Notice that renormalizing a J term entangles two neighboring spins, while the renormalization of a Γ term freezes that spin along the direction of the magnetic field, and decouples it from the chain.

It can be shown that the fusion rules of Majorana fermions correspond to the $SU(2)_{k=2}$ algebra, which in turn coincide with those of the quantum group $U_{q=i}(su(2))$ with the relation $q = e^{i2\pi/(k+2)}$ [58–62]. The nonunivocal fusion rule

$$\frac{1}{2} \times \frac{1}{2} = 0 + 1, \tag{8}$$

corresponds to the pairing of two Majorana fermions, for instance $\alpha_m \beta_m$, which in terms of of Dirac fermions is $2(c_m^\dagger c_m - 1/2)$, see Eq. (3), and we can attach the fusion channel 0 (1) to the -1 ($+1$) eigenvalue. Indeed, notice that Eq. (8) reminds the composition of two $1/2$ spins. Thus we may call the less energetic channel a *generalized singlet state* [62,63], and the other channel as a *generalized triplet* (albeit there is no S_z degeneracy). Notice that while the $1/2$ spins obey the SU(2) algebra and the singlet states span the total $S_z = 0$ Hilbert space sector, Majorana fermions obey the $SU(2)_{k=2}$ algebra and the generalized singlet state spans the Hilbert space sector for the fusion channel 0.

With this parallelism in mind, we can devise an SDRG specially suited for an inhomogeneous Majorana chain [64,65], as it is done in Appendix A. At each RG step, the two Majorana fermions linked through the strongest coupling (notice that in terms of Majorana fermions the J and Γ terms are equivalent) are fused into their less energetic channel, forming a generalized singlet state or *bond*, and leaving a renormalized coupling between their closest neighbors. This scheme is completely equivalent to Fisher's RG, Eqs. (6) and (7). In this case, the SDRG becomes analogous to the Dasgupta-Ma technique for spin-1/2 XX chains [30], for which it can be proved that the bonds never cross [35].

Let us apply this RG scheme to the Majorana Hamiltonian given in Eq. (4). The first Majorana pair to be decimated is $(\beta_{-1/2}, \alpha_{1/2})$, because $J_{-1/2}$ is the strongest coupling. Hence, these two Majorana fermions fuse into a Dirac fermion,

$$b_{1/2} = \tfrac{1}{2}(\beta_{-1/2} + i\alpha_{1/2}), \tag{9}$$

which becomes decoupled. Using Eq. (7) we can find an effective Hamiltonian with $2(N-1)$ Majorana fermions, whose new central term $\tilde{\Gamma}_{1/2}\alpha_{-1/2}\beta_{1/2}$ is given by

$$\tilde{\Gamma}_{1/2} = \frac{\Gamma_{-1/2}\Gamma_{1/2}}{J_{-1/2}} = e^{-\frac{3h}{2}}. \tag{10}$$

The strongest coupling is now $\tilde{\Gamma}_{1/2}$. We apply the RG again, and the decimated Majorana fermions fuse into a Dirac fermion,

$$d_{1/2} = \tfrac{1}{2}(\alpha_{-1/2} + i\beta_{1/2}). \tag{11}$$

The new effective Hamiltonian of $2(N-2)$ Majorana fermions has a central term $\tilde{J}_{3/2}$ which is given by Eq. (6),

$$\tilde{J}_{3/2} = \frac{J_{-3/2}J_{1/2}}{\tilde{\Gamma}_{1/2}} = e^{-\frac{5h}{2}}, \tag{12}$$

which is again the strongest coupling in the chain. Given the symmetry of the coupling constants, Eq. (5), all RG steps decimate the central pair of Majorana fermions, fusing them alternatively into b and d Dirac fermions. Hence, the ground state, that we shall call the Majorana rainbow state $|\mathrm{MRS}\rangle$, is annihilated by the following Dirac operators:

$$b_m |\mathrm{MRS}\rangle = 0, \quad d_m |\mathrm{MRS}\rangle = 0, \quad m = \tfrac{1}{2}, \ldots, L - \tfrac{1}{2}, \tag{13}$$

with

$$b_m = \tfrac{1}{2}(\beta_{-m} + i\alpha_m), \quad d_m = \tfrac{1}{2}(\alpha_{-m} + i\beta_m). \tag{14}$$

$|\mathrm{MRS}\rangle$ is a concentric generalized singlet state, shown in Fig. 2.

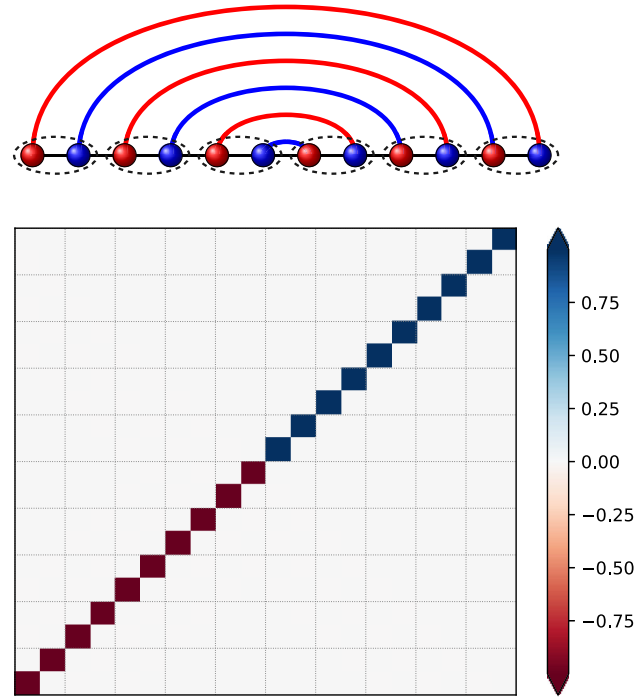

FIG. 2. Top: schematic representation of the outcome of the RG for a chain of six spins. Blue bonds stand for b-type Dirac fermions, while red ones represent d-type fermions, see Eq. (14), which can also be considered as generalized singlet states corresponding to the less energetic fusion channel. Bottom: covariance matrix of the RS for $N = 20$ and $h = 10$. Notice that the nonzero elements are in the antidiagonal, as it is dictated by the structure of the b and d fermions.

It is worth to compare the Majorana rainbow state Eq. (13) with its Dirac counterpart, which emerges as the GS of the inhomogeneous XX chain and its fermionic version [32,34–36]. This state can be seen as a singlet state of concentric bonding and antibonding operators,

$$|\mathrm{RS_{XX}}\rangle = \prod_{m=1/2}^{L-1/2} (b_m^-)^\dagger (b_m^+)^\dagger |0\rangle, \tag{15}$$

with

$$\begin{cases} b_m^+ = \frac{1}{\sqrt{2}}(c_m + c_{-m}) \\ b_m^- = \frac{1}{\sqrt{2}}(c_m - c_{-m}) \end{cases}. \tag{16}$$

The alternation between bonding and antibonding is due to the nonlocal nature of the Jordan-Wigner transformation, since

each long-distance coupling acquires a phase related to the number of fermions contained in it. In spin language, the XX model $|RS_{\rm XX}\rangle$ is formed by spin-1/2 concentric singlets. The alternation between bonding and antibonding in Eq. (15) is therefore similar to that of b and d Dirac fermions in Eq. (14).

Let us compute the EE of a subsystem A, with length L_A, for the Majorana RS, Eq. (13). The EE of any partition of a ground state formed by SU(2) singlet states can be estimated by counting the number of bonds which cross the partition boundary, and multiplying by ln(2). The procedure is the same when we deal with generalized singlet states. The EE of any subsystem A can be estimated by counting the number of bonds which cross the partition boundary and multiplying by $\ln d$ [62], where $d=\sqrt{2}$ is the quantum dimension of the spin 1/2 representation of the algebra $SU(2)_2$.

Alternatively, the EE of a Gaussian state can be obtained from its covariance matrix (CM), $\mathcal{C}$,

$$\mathcal{C}_{ab}=\langle[\gamma_a,\gamma_b]\rangle, \tag{17}$$

where we have arranged the Majorana operators in a vector form $\boldsymbol{\gamma}^T=(\alpha_{-L+1/2},\beta_{-L+1/2},\ldots,\alpha_{L-1/2})$. In Appendix B we provide a brief derivation of this expression. The structure of the GS obtained through the decimation procedure shows up in the CM, as we can see in Fig. 2(b). The EE of a subsystem A with size L_A can be computed through the eigenvalues $\pm\lambda_k$, $k\in\{1,\cdots,L_A/2\}$ of the appropriate restriction $\mathcal{C}_A$ of the CM [66], through

$$S_A=-\sum_{k=1}^{L_A}\nu_k\ln\nu_k,\quad \nu_k=\frac{1}{2}(1+\lambda_k). \tag{18}$$

We can now compute the EE of a lateral block of the system, $A_\ell=\{-L+1/2\cdots-L+1/2+2\ell\}$, with $\ell=1,\cdots,L$. Notice that a block with an odd number of Majorana operators has no physical sense. Thus A_ℓ must contain an even number of Majorana fermions, which correspond to the physical fermions (dotted boxes) or the spins (black balls) of Fig. 1. We can obtain the EE by counting the number of bonds n_b (reds and blues) that A_ℓ cuts in Fig. 2 and multiply it by $\ln d$.

$$S_A=n_b\ln\sqrt{2}. \tag{19}$$

Hence, we have that the EE of the MRS grows linearly,

$$S(A_\ell)=2\ell\ln\sqrt{2}=\ell\ln 2, \tag{20}$$

and the maximal EE corresponds to the half chain block $S(A_L)=L\ln 2$.

B. Weak inhomogeneity regime

In this section, we shall consider the GS of Eq. (2) with couplings given by Eq. (5), in the low inhomogeneity regime, $h\ll 1$. The equations of motion associated to the lattice Hamiltonian in the Heisenberg picture are given by $i\partial_t\alpha_{\pm m}=[H,\alpha_{\pm m}]$ and $i\partial_t\beta_{\pm m}=[H,\beta_{\pm m}]$. Using Eq. (4), we have

$$\begin{aligned}\partial_t\alpha_n&=-2e^{-2h|n|}(\beta_n-e^{{\rm sign}(n)h}\beta_{n-1}),\\ \partial_t\beta_n&=2e^{-2h|n|}(\alpha_n-e^{{\rm sign}(n)h}\alpha_{n+1}).\end{aligned} \tag{21}$$

Now, we define the fields

$$\alpha_m=\sqrt{a}\alpha(x),\quad \beta_m=\sqrt{a}\beta(x), \tag{22}$$

where a is the lattice spacing between the Dirac fermions c_m, $x=ma$, which satisfy the usual anticommutation relations, $\{\alpha(x),\alpha(x')\}=\{\beta(x),\beta(x')\}=2\delta(x-x')$ and $\{\alpha(x),\beta(x)\}=0$. We find the continuum limit of the lattice equations of motion by plugging these fields into Eqs.(21) and requiring $a\to 0$ and $L\to\infty$ with both $\mathcal{L}=aL$ and $\hat{h}=h/a$ kept constant,

$$\begin{aligned}\partial_t\alpha(t,x)&\approx-2ae^{-2\hat{h}|x|}(\partial_x-{\rm sign}(x)\hat{h})\beta(t,x),\\ \partial_t\beta(t,x)&\approx-2ae^{-2\hat{h}|x|}(\partial_x-{\rm sign}(x)\hat{h})\alpha(t,x),\end{aligned} \tag{23}$$

where we made the approximation $e^{{\rm sign}(x)h}\approx(1+{\rm sign}(x)h)$. If $h=0$ the equations of motion (23) correspond to the massless Dirac equation $i\partial\!\!\!/\Psi=(i\gamma^0\partial_0+i\gamma^1\partial_1)\Psi=0$, where we have introduced the spinor

$$\Psi^T=(\alpha(x^0,x^1),\beta(x^0,x^1)),\quad (x^0,x^1)=(2t,x). \tag{24}$$

Our choice for the γ matrices is $\gamma^0=-\sigma_2$, $\gamma^1=i\sigma_3$ and $\gamma^3=\sigma_1$, where σ_i, $i=1,2,3$, are the Pauli matrices. Hereafter, we choose $a=1$ that sets the Fermi velocity $v_F=1$, so we can simplify $\hat{h}=h$, $\mathcal{L}=L$, and rewrite the equations of motion of the inhomogeneous system, Eq. (23), as

$$(-\sigma_2\partial_0+e^{-2h|x^1|}i\sigma_3(\partial_1-{\rm sign}(x^1)h))\Psi=0. \tag{25}$$

The previous equation corresponds to the massless Dirac equation in a curved space-time whose metric depends on the inhomogeneity h, see Appendix C for details. The Dirac equation on a generic metric can be written as Eq. (C5),

$$\left(-\sigma_2\partial_0+\frac{i}{2}\omega_0^{01}\sigma_3+\frac{E_1^1}{E_0^0}\left(i\sigma_3\partial_1-\frac{i}{2}\omega_1^{01}\sigma_2\right)\right)\Psi=0, \tag{26}$$

where ω_μ^{ab} is the spin connection and E_a^μ is the inverse of the *zweibein*. Comparing Eq. (26) with our equations of motion Eq. (25), we obtain

$$\frac{E_1^1}{E_0^0}=e^{-2h|x^1|}, \tag{27}$$

$$\omega_0^{01}=-2e^{-2h|x^1|}h{\rm sign}(x^1), \tag{28}$$

$$\omega_1^{01}=0. \tag{29}$$

The solution of these equations gives rise to the space-time metric:

$$g_{00}=-e^{-4h|x|},\quad g_{11}=1, \tag{30}$$

whose Euclidean version is

$$ds^2=e^{-4h|x|}dt^2+dx^2=\Omega^2(x)dzdz, \tag{31}$$

where $\Omega(x)=e^{-2h|x|}$ is the Weyl factor and

$$z=\tilde{x}+it,\quad \text{with}\quad \tilde{x}=\int_0^x\frac{dy}{\Omega(y)}=\frac{{\rm sign}(x)}{2h}(e^{2h|x|}-1). \tag{32}$$

The nonzero Christoffel symbols are

$$\Gamma^0_{01}=-2h{\rm sign}(x),\quad \Gamma^1_{00}=-2h{\rm sign}(x)e^{-4h|x|}, \tag{33}$$

and the nonzero components of the Ricci tensor are

$$R_{00}=-e^{-4h|x|}(4h\delta(x)-4h^2),\quad R_{11}=4h\delta(x)-4h^2. \tag{34}$$

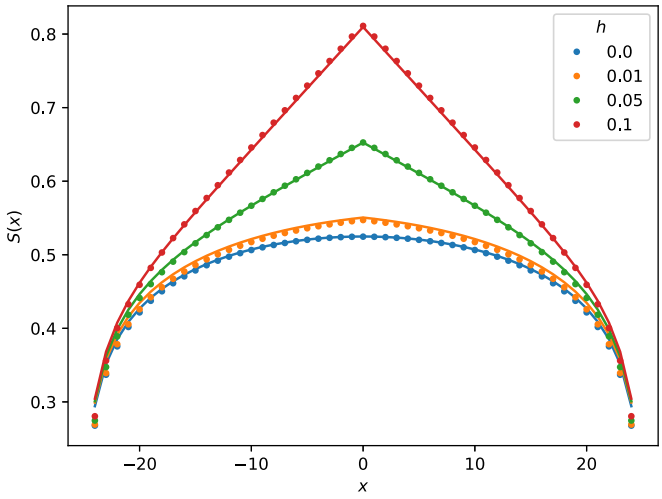

FIG. 3. EE of lateral blocks of the GS of Eq. (2) with couplings (5) for different values of h and $L = 40$. The dots represent the numerical values obtained by exact diagonalization and the lines correspond to the predictions of Eq. (36) using Eq. (D3).

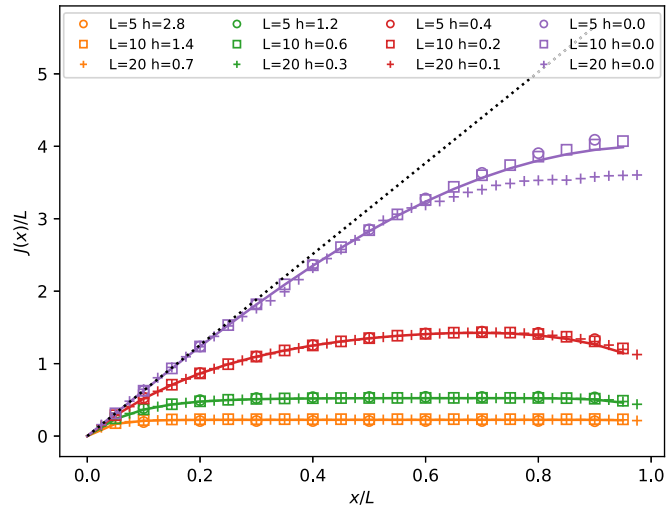

FIG. 4. Normalized weight functions $J(x)/L$ determining the EH for different values of $\lambda = 2hL$. Continuous lines correspond to the theoretical prediction, Eq. (39). The dotted black straight line corresponds to the Bisognano-Wichmann prediction for a semi-infinite system.

The scalar of curvature $R = g^{\mu\nu}R_{\mu\nu}$ is

$$R = 8(h\delta(x) - h^2), \tag{35}$$

where we have used Eq. (30). Thus R is singular at the origin and constant and negative everywhere else, thus allowing for the holographic interpretation of the rainbow state that has been discussed in the literature [38].

1. Entanglement entropies

We have shown that the continuum limit of the lattice model Eq. (4) corresponds to a Majorana field in curved space-time, described by a conformal field theory with central charge $c = 1/2$. We can obtain the EE of a block within this state employing standard procedures [12], via the correlation function of twist operators in an n-times replicated world-sheet. The EE in the curved background is related to the one in flat space through the Weyl transformation of the twist operators. Hence, the EE of the lateral blocks considered in the previous section is (see details of the derivation in Ref. [36]):

$$S(x) = \frac{1}{12}\ln\left(\Omega(x)\frac{8\tilde{L}}{\pi}\cos\left(\frac{\pi\tilde{x}}{4\tilde{L}}\right)\right) + c_I'(\tilde{x}), \tag{36}$$

where the deformed quantities, $\tilde{x}$ and $\tilde{L}$, are computed using Eq. (32). The nonuniversal function $c_I'(\tilde{x})$ can be found using the relation between the EEs of an XX chain of length $2L$ and an ITF chain of length L [67], and is given in Eq. (D3) of Appendix D. Figure 3 shows the numerical values of the EE for different values of h, showing the agreement with Eq. (36). In the limit $hL \gg 1$, Eq. (36) implies for the half chain

$$S(x = 0) \approx \frac{1}{6}hL, \tag{37}$$

which scales linearly with the system size, thus presenting a smooth crossover between the weak and the strong inhomogeneity regimes for which the EE is given by Eq. (20), i.e., $S_{A_L} = L\ln 2$. In addition, this value of the EE can be interpreted as that of a thermal state with an effective temperature h/π [36].

2. Entanglement Hamiltonian

Let us now characterize the EH associated to the reduced density matrix of the half chain, that we shall denote $\mathcal{H}_L$. In Appendix E, we discuss the standard procedure to obtain the EH using the covariance matrix C_L [46,66]. The EH describes a local inhomogeneous system with the weakest couplings near the center, which is the internal boundary between the block and its environment. Moreover, if the physical system is critical and infinite, it can be shown that $\mathcal{H}_L$ is given by [47]

$$\mathcal{H}_L = 2\pi L\int_0^L dx\, J(x)\, T_{00}(x), \tag{38}$$

where $T_{00}(x)$ is the Hamiltonian density of the physical system and $J(x)$ is a weight function. The Bisognano-Wichmann theorem predicts $J(x) \approx x$ for a semi-infinite line [44,45], thus being approximately applicable for our case. Moreover, when the original system is placed on a static metric, the weight function in Eq. (38) $J(x)$ should be appropriately deformed following Eq. (32) [37]. In our case, we obtain

$$J(x) = \frac{2L}{\pi}\frac{e^{\lambda}-1}{\lambda}e^{-\lambda\frac{x}{L}}\sin\left(\frac{\pi}{2}\frac{e^{\lambda\frac{x}{L}}-1}{e^{\lambda}-1}\right), \tag{39}$$

where $\lambda = 2hL$. Near the internal boundary, which corresponds to the center of the chain, the weight function $J(x)$ grows linearly $J(x) \simeq 2\pi x$, as predicted by Bisognano and Wichmann [44,45]. Far from $\tilde{x} = 0$, the weight function develops a plateau, as it can be seen in Fig. 4 where $J(x)$ is plotted for different values of λ.

III. OUT OF CRITICALITY

Let us consider an inhomogeneous ITF model described by the Hamiltonian (2) or, equivalently, Eq. (4), with a modifica-

tion of the coupling constants Eq. (5) studied in the previous section,

$$J_m = \begin{cases} e^{-2h|m+1/2|+\delta} & \text{if } m \neq -1/2, \\ e^{-h/2+\delta} & m = -1/2, \end{cases} \tag{40}$$

$$\Gamma_m = e^{-2h|m|-\delta}, \tag{41}$$

where $\delta \in \mathbb{R}$. Notice that if $h = 0$ and $\delta \ll 1$, then $J_m = 1 + \delta$ and $\Gamma_m = 1 - \delta$, and our system describes a Majorana chain with alternating couplings, thus showing a relation to the Kitaev chain and the Su-Schrieffer-Heeger (SSH) model describing a dimerized chain of Dirac fermions [68,69]. Indeed, the alternating term $e^{\pm\delta}$ pushes the system described in Sec. II out of criticality, as we will describe throughout this section.

A. Strong inhomogeneity

Let us consider the Hamiltonian given in Eq. (4) in the limit $h \gg 1$. We can apply the same SDRG of the previous section, making use of the parameter

$$\kappa = \delta/h. \tag{42}$$

The RS is obtained when all the RG steps decimate the Majoranas at the center of the chain, but we will show that other structures may be obtained, depending on the value of κ. In order to decimate the central pair we need $J_{1/2}$ to be the strongest coupling of the chain. In other words, $J_{-1/2} > \Gamma_{1/2}$ which implies that $e^{-h(1/2-\kappa)} > e^{-h(1+\kappa)}$. Hence, we arrive at the condition

$$\frac{1}{2} - \kappa < 1 + \kappa \Rightarrow \kappa > -\frac{1}{4}. \tag{43}$$

Thus, if $\kappa > -1/4$ the Majorana fermions $\beta_{-1/2}$ and $\alpha_{1/2}$ fuse into the Dirac fermion $b_{1/2}$, defined in Eq. (9) and, using Eq. (7), we obtain a renormalized coupling

$$\tilde{\Gamma}_{1/2} = e^{-3h\left(\frac{1}{2}+\kappa\right)}, \tag{44}$$

which will couple $\alpha_{-1/2}$ and $\beta_{1/2}$. These Majorana fermions are decimated at the second RG step fusing into $d_{1/2}$, Eq. (11), if $\tilde{\Gamma}_{1/2} > J_{1/2}$, implying that

$$3\left(\frac{1}{2} + \kappa\right) < 2 - \kappa \Rightarrow \kappa < \frac{1}{8}, \tag{45}$$

and then a new term appears in the effective Hamiltonian of the form $\tilde{J}_{3/2}\beta_{-3/2}\alpha_{3/2}$, where $\tilde{J}_{3/2}$ follows from Eq. (6),

$$\tilde{J}_{3/2} = e^{-5h\left(\frac{1}{2}-\kappa\right)}. \tag{46}$$

Summarizing, the first central decimation requires $\kappa > -1/4$ while the second requires $\kappa < 1/8$. We can iterate this procedure and find that the bound on κ associated with exactly n consecutive central decimations is given by

$$\begin{aligned} \kappa &> -\frac{1}{4n}, \text{ if } n \text{ odd}, \\ \kappa &< \frac{1}{4n}, \text{ if } n \text{ even}. \end{aligned} \tag{47}$$

The state with exactly n central decimations will be called $|n\rangle$. With this notation, the RS corresponds to $|n = 2L\rangle$, and satisfies

$$|\kappa| < \frac{1}{8L}. \tag{48}$$

Whenever a central decimation fails, the SDRG must choose the strongest couplings between two identical links, symmetrically placed with respect to the center of the chain. That is not a problem for the algorithm, because the links are not consecutive [40]. More relevantly, from that moment on the RG will always proceed by *dimerizing* the chain towards the extremes, except perhaps for a final long distance bond, depending on the parity of the system, related to the Kitaev phase [50].

Thus we are led to the following physical picture, which is illustrated in Fig. 5. In panel (a) we can see the GS for $\kappa < -1/4$. No central bonds are created, and we obtain the state $|n = 0\rangle$. Panel (b) shows the GS for $\kappa > 1/8$, in which a single central bond is created. Due to parity reasons, a second bond must appear between the extremes of the chain, thus leading to the nontrivial Kitaev chain, which we call the state $|n = 1\rangle$. Panel (c) shows the state $|n = 4\rangle$ and panel (d) the state $|n = 3\rangle$, which can be obtained within fixed ranges of $\kappa \in (-1/12, -1/20)$ and $\kappa \in (1/24, 1/16)$ respectively, which can be found through Eq. (47).

This physical picture can be confirmed through the analysis of the covariance matrices, which are depicted using a color code in Fig. 6. Indeed, we can see the CM for $N = 20$ spins and $h = 10$, in the suitable range for $|n = 4\rangle$ (left) and $|n = 5\rangle$ (right). The central patterns show $n = 4$ and $n = 5$ central arcs, respectively. As predicted, the $n = 5$ case presents an extra bond between the extremes of the system, showing that it belongs to the nontrivial Kitaev phase.

Furthermore, we examine the EE of lateral blocks, $S(A_\ell)$ in the top panel of Fig. 7, which has been computed from the CM using the same systems, with $N = 10$ spins and $h = 10$. As predicted in our physical picture, the EE for the smallest block begins at 0 or $\ln(2)$ depending on the sign of κ, and presents a linear tent-shape at the center, within a block of $\lfloor n/2 \rfloor$ spins and reaching an EE $n\ln(2)/2$. The topological nature of the states is clarified in Appendix F, where we present a graphical way to distinguish the trivial and topological phases by overlaying each state with the trivial state $|n = 0\rangle$ and counting the total number of loops.

We can also consider the energy gap around the Fermi level to capture the differences between ground states. Defining the energy gap in an inhomogeneous system presents some challenges, since it should be expressed in units of the typical energy scale. A strategy that has proved useful in similar cases is to rescale the energy gap with the lowest coupling of the system [40], which in this case becomes $\Gamma_{L-1/2} \approx e^{-2hL}$. Hence, the scaled gap

$$\hat{\Delta}^{(0)} \equiv \frac{E_{N+1} - E_N}{\Gamma_{L-1/2}}, \tag{49}$$

becomes constant ($\hat{\Delta}^{(0)} = 2$), as it can be seen in Fig. 7(b). The states $|n \text{ odd}\rangle$ present a zero mode at the edge, and the system is strictly gapless, $\hat{\Delta}^{(0)} = 0$. Therefore it is convenient to consider the second gap, defined as

$$\hat{\Delta}^{(1)} \equiv \frac{E_N - E_{N-1}}{J_{L-1/2}}, \tag{50}$$

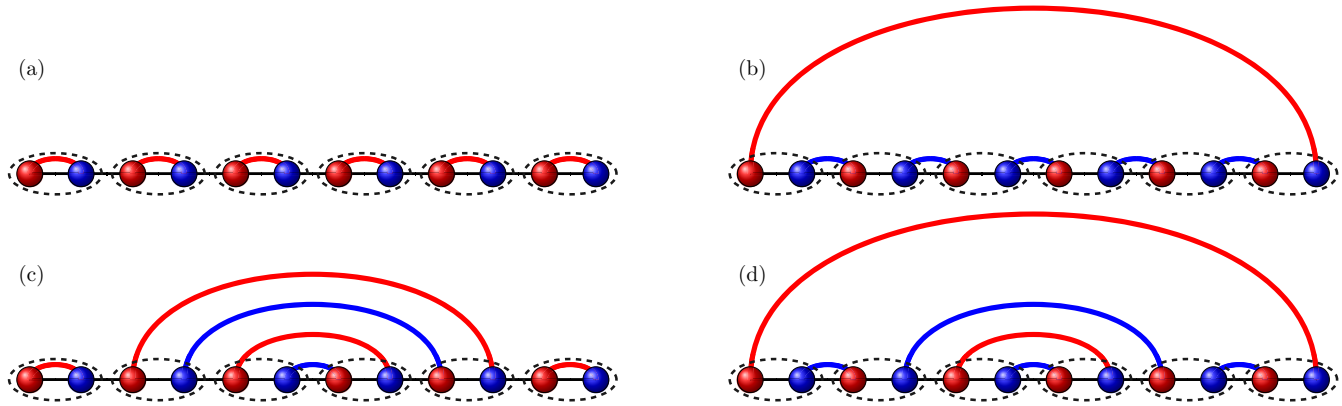

FIG. 5. Schematic representation of different ground states of Eq. (4) obtained with the SDRG scheme. The trivial (a) and nontrivial (b) local pairings correspond to the states $|n=0\rangle$ and $|n=1\rangle$, the two possible ground states of the Kitaev chain. (c) and (d) illustrate ground states with coexistence between nonlocal rainbowlike and local fermions. The topological type of the local pairing depends on the parity of n. Hence, we have a trivial pairing (c) $|n=4\rangle$ and a non trivial one $|n=3\rangle$ in (d).

which can also be seen in Fig. 7(b). If $n \leqslant (2L-3)$, there is a short-range Majorana singlet state and the gap is finite, $\hat{\Delta}^{(1)} = 2$. Yet, both gaps fall to zero for the rainbow state, $|n=N\rangle$.

B. Weak inhomogeneity

Proceeding in the same way as in the previous section, we can obtain the equations of motion from the Hamiltonian (4) and describe the continuum limit defining $x = am$, $a \to 0$, $h \to 0$, with $\hat{h} = h/a$ and $\mathcal{L} = La$ kept constant, in terms of the fields $\alpha(x,t)$ and $\beta(x,t)$,

$$\begin{aligned}\partial_t \alpha &\approx -2ae^{-2\hat{h}|x|}(ae^{\delta}\partial_x - (\mathrm{sign}(x)he^{\delta} + 2\sinh\delta))\beta,\\ \partial_t \beta &\approx -2ae^{-2\hat{h}|x|}(ae^{\delta}\partial_x - (\mathrm{sign}(x)he^{\delta} - 2\sinh\delta))\alpha,\end{aligned} \quad (51)$$

where we will use $a = 1$ for convenience. These equations can be rewritten in terms of a spinor field Ψ, Eq. (24), using the same γ matrices, obtaining

$$\begin{aligned}(-\sigma_2\partial_0 + e^{-2h|x^1|}(i\sigma_3 e^{\delta}\partial_1\\ - i\sigma_3 \mathrm{sign}(x^1)he^{\delta} + 2i\sinh\delta))\Psi = 0,\end{aligned} \quad (52)$$

And, then, we can compare this equation with that representing the dynamics of a Dirac field in a curved space-time:

$$\left(-\sigma_2\partial_0 + \frac{i}{2}\omega_0^{01}\sigma_3 + \frac{E_1^1}{E_0^0}\left(i\sigma_3\partial_1 - \frac{i}{2}\omega_1^{01}\sigma_2\right) + i\frac{m}{E_0^0}\right)\Psi = 0. \quad (53)$$

where ω_μ^{ab} is again the spin connection and E_a^μ the inverse of the *zweibein*. From the above identification we find that

$$\begin{aligned}E_0^0 &= e^{2h|x^1|}, \quad E_1^1 = e^{\delta},\\ \omega_0^{01} &= -2e^{-2h|x^1|}e^{\delta}h\mathrm{sign}(x^1),\\ \omega_1^{01} &= 0,\\ m &= 2\sinh\delta,\end{aligned} \quad (54)$$

that leads to a (1+1)D metric whose nonzero terms are

$$g_{00} = -e^{-4h|x|}, \qquad g_{11} = e^{-2\delta}. \quad (55)$$

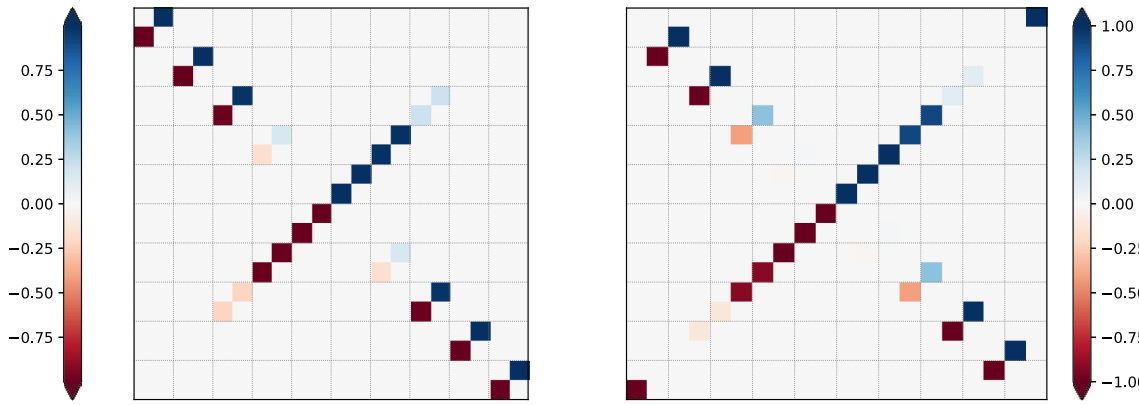

FIG. 6. Covariance matrices of states $|n=4\rangle$ and $|n=5\rangle$ for $h=10$ and $N=20$. The short-range single states populate the secondary diagonals while the long-range singlet states correspond to the antidiagonal.

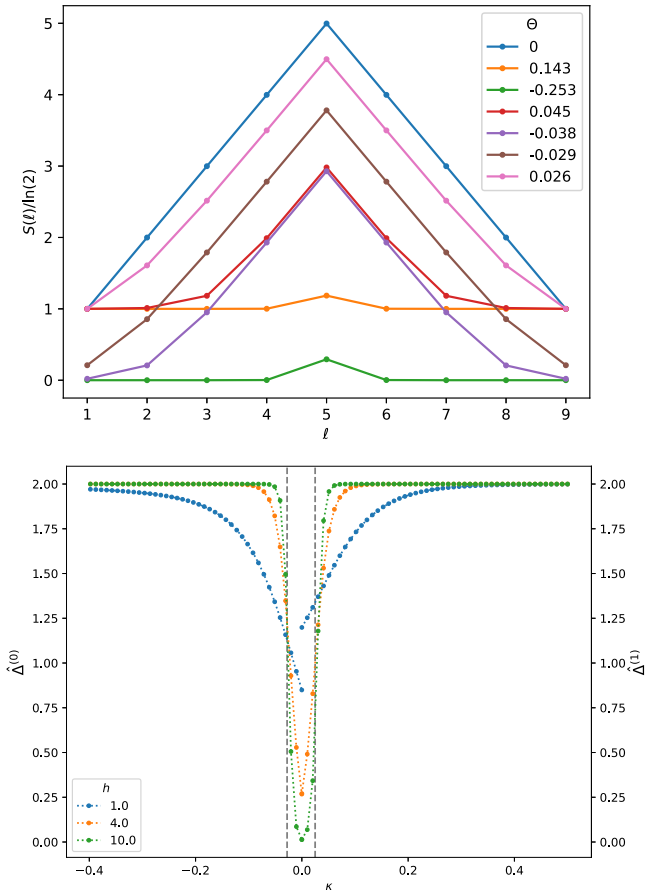

FIG. 7. (Top) EE of lateral blocks of a chain of $N = 10$ spins for different values of κ, using $h = 10$. For $\kappa = -0.33$ and 0.14, we obtain respectively the $|n = 0\rangle$ and $|n = 1\rangle$ states, for which the entropy is flat. On the other extreme, the $\kappa = 0$ curve corresponds to the rainbow state, $|n = 10\rangle$, which presents maximal EE growth. The intermediate values of κ are chosen following Eq. (47) and present different numbers of central bonds. The EE for the half-chain, $\ell = 5$, agrees with Eq. (19). (Bottom) Scaled energy gaps ($\hat{\Delta}^{(0)}$ for $\kappa < 0$ and $\hat{\Delta}^{(1)}$ for $\kappa > 0$) of the same chain for different values of h. The vertical gray lines delimit the rainbow state region for this chain size ($n > 2(L-1)$).

However, $g_{11} \simeq 1$ if $\delta \ll 1$, and thus the associated metric coincides with the one found in the previous section, see Eq. (31). Thus the field theory associated with the system described by the Hamiltonian (4) is described by a massive Majorana fermion, with $m \approx 2\delta$, placed in the curved background described by the metric Eq. (31).

1. Entanglement entropies

Let us first consider the case $h = 0$, i.e., the massive fermion on a flat space. The EE of this system has been obtained previously by evaluating the associated two-dimensional classical model via the CTM formalism [46]. For $\delta > 0$, one obtains

$$S(\delta) = \frac{1}{12}\left(\ln\left(\frac{k^2}{16k'^2}\right) + \left(1 - \frac{k^2}{2}\right)\frac{4I(k)I(k')}{\pi}\right) + \ln 2, \tag{56}$$

while for $\delta < 0$ we get

$$S(\delta) = \frac{1}{12}\left(\ln\left(\frac{4}{kk'}\right) + \frac{1}{2}(k^2 - k'^2)\frac{4I(k)I(k')}{\pi}\right), \tag{57}$$

where $I(x)$ is the complete elliptic integral of the first kind [70] and

$$k = e^{-2|\delta|}, \qquad k' = \sqrt{1 - k^2}. \tag{58}$$

Notice that if $|\delta| \ll 1$, $k \approx (1 - |\delta|)/(1 + |\delta|)$ which is the value used in Refs. [46,49]. Although Eq. (57) is only exact for the infinite chain, it is still valid provided that $1/\delta \ll L$, i.e., when the cluster decomposition principle is satisfied. Near the critical point, $\delta \ll 1$, Eqs. (57) are simplified to

$$S \approx \frac{c}{6}\ln\left(\frac{1}{1-k}\right) = \frac{c}{6}\ln\xi, \tag{59}$$

where the quantity inside the logarithm can be interpreted as a correlation length ξ [12] with the appropriate units of length,

$$\xi = \frac{1}{1-k} \approx \frac{1}{2|\delta|}, \tag{60}$$

which corresponds to the inverse of the mass, $m = 2\delta$, Eq. (54). To end this brief summary of the homogeneous non critical case, let us write the EE for the half chain of a *finite* system as

$$S(\delta, L) = \frac{c}{6}\ln\frac{\xi_E(\delta, L)}{2} + b(\delta), \tag{61}$$

where $\xi_E(\delta, L)$ shall be called the *entangled length*, because it plays the role of an effective correlation length in order to compute the EE, even though its value is upper bounded by the size of the system, $N = 2L$. If $\delta = 0$, the system is critical and $\xi_E(0, L)$ saturates this bound, thus leading to the logarithmic scaling predicted by CFT. On the other hand, if $|\delta|$ is large enough then $\xi_E(\delta, L) \ll 2L$, finite-size effects are not important and the cluster decomposition principle holds. Thus the results for the infinite chain can be applied, and the area law is satisfied. Hence, we see that in this case Eq. (61) is just a reparametrization of Eq. (57).

Moreover, when we introduce inhomogeneity in the system through the parameter h, we find that the EE can be obtained merely *deforming* the entangled length $\xi_E(\delta, L)$ according to the same prescription used before, given in Eq. (32), giving rise to the ansatz

$$S(L, \delta, h) = \frac{c}{6}\ln(\tilde{\xi}_E(\delta, L)) + b(\delta), \tag{62}$$

where

$$\tilde{\xi}_E(h, \delta, L) = \frac{1}{2h}(e^{h\xi_E(\delta,L)} - 1), \tag{63}$$

is the deformed entangled length, corresponding to the curved space-time.

We have fitted expression Eq. (62) to the numerical values for the EE of the half chain for different values of δ and h, using $\xi_E(\delta, L)$ and $b(\delta)$ as fitting parameters. The agreement between the fits and the numerical results can be seen in the top panel of Fig. 8. Hence, we obtain a single value for the entangled length for each L and δ, which accounts for the EE under different degrees of inhomogeneity h. In the bottom panel of Fig. 9 we can see the good agreement between the

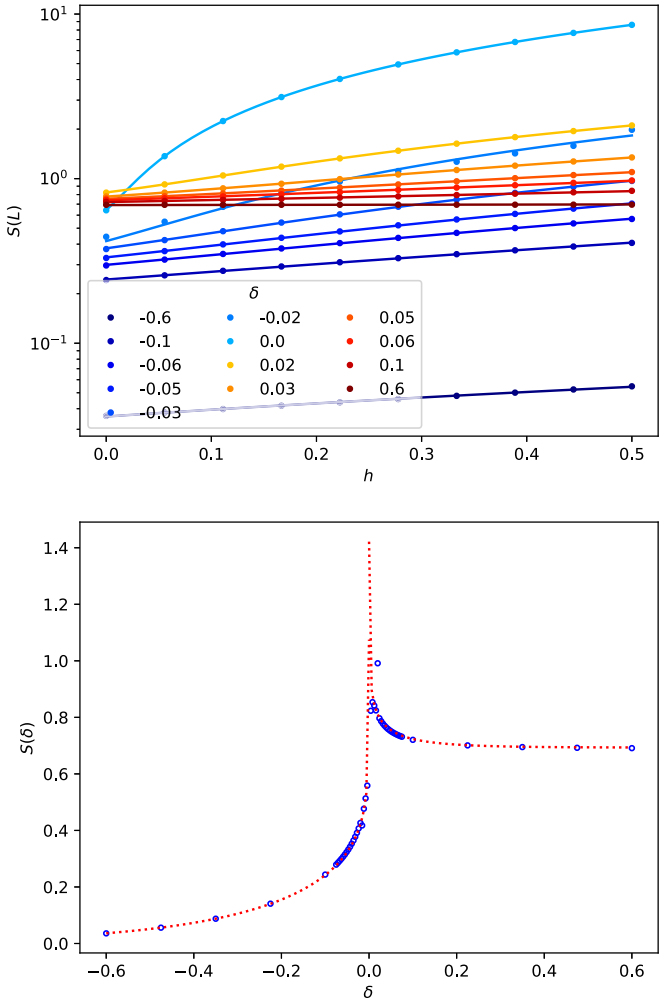

FIG. 8. (Top) Plot of the fits (lines) performed with expression (63) of the numerical results for the half chain EE (points) for different values of δ. (Bottom) The dotted red line corresponds to Eq. (57) and the blue dots to Eq. (62), where $\xi_E(\delta, L)$ has been obtained by fitting Eq. (63) to the numerical half chain EE of a system with $L = 100$.

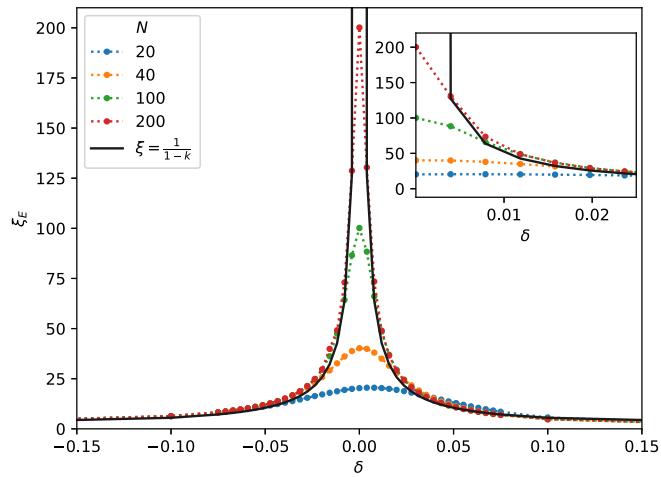

FIG. 9. Entanglement correlation length $\xi_E(\delta, L)$ for different chain sizes $2L$. Near the critical point we have $\xi_E \approx \xi$, Eq. (60).

infinite chain prediction, Eq. (57), and the output of Eq. (61) having used the values $\xi_E(\delta, L)$ and $b(\delta)$ that were obtained from the previous fits.

In Fig. 9, we present the fitted values $\xi_E(\delta, L)$ for different system sizes. The system presents universal behavior as long as the correlation length is much smaller than the system size.

It is worth to ask whether the weak and strong inhomogeneity regimes match smoothly. Let us consider the limit $h \gg 1$ in Eq. (62),

$$S(L, \delta, h) \approx \frac{c}{6} h \xi_E(\delta, L). \tag{64}$$

If $\delta = 0$ we have $S(L, 0, h) \approx \frac{c}{3} hL$, as it was discussed in the previous section. On the other hand, if $\delta \ll 1$ but $1/\delta \ll L$, $\xi_E(\delta, L) = \xi$ from Eq. (60). Hence,

$$S(L, \delta, h) \approx \frac{h}{12\delta} = \frac{1}{12\kappa}, \tag{65}$$

which is a manifestation of the area law given by the interplay between the inhomogeneity h and the dimerization δ. Thus we see that the weak and strong inhomogeneity regimes match.

2. *Entanglement Hamiltonian and entanglement spectrum*

The reduced density matrix ρ_A of a half infinite chain can be written in terms of the generator of the Baxter corner matrix,

$$\rho_A = e^{-H_{CTM}}, \tag{66}$$

Since the model is integrable, we can simplify and state that $H_{CTM} = \epsilon H_{\mathcal{N}}$, where $H_{\mathcal{N}}$ is a Hermitian operator with integer spectrum. Thus the ES ϵ_l, with $l = 1, \ldots, L$, is equally spaced and we may focus on the level spacing ϵ. For the ITF model we have

$$\epsilon = \pi \frac{I(k')}{I(k)}, \tag{67}$$

where k and k' are given by Eq. (58). The EH of the half infinite chain can be identified with the generator of the CTM [49]. Thus, in the case of the ITF chain, the first neighbor couplings grow linearly from the internal boundary towards the bulk with a parity oscillation between 1 and k,

$$\mathcal{H} = \sum_{l=1}^{\infty} J^{EH}_{2\ell-1} \alpha_\ell \beta_\ell + J^{EH}_{2\ell} \beta_\ell \alpha_{\ell+1}, \tag{68}$$

with

$$\begin{aligned} J^{EH}_{2\ell-1} &= I(k')(2\ell - 1), \quad J^{EH}_{2\ell} = I(k')2\ell k, \quad \delta < 0, \\ J^{EH}_{2\ell-1} &= I(k')(2\ell - 1)k, \quad J^{EH}_{2\ell} = I(k')2\ell, \quad \delta > 0, \end{aligned} \tag{69}$$

where α_ℓ and β_ℓ correspond to the lattice Majorana fermions. Figure 10(a) shows the nearest neighbor coupling constants of the EH, J^{EH}_ℓ, slightly modified in order to improve the visualization: for odd values of ℓ, J^{EH}_ℓ has been divided by k in order to remove the parity oscillation, leaving a linear growth with slope $2I(k')$, in similarity to Ref. [49]. If we switch on the inhomogeneity, setting $h = 0.5$, we can observe the same EH couplings in Fig. 10(b): a linear increase of the couplings with a parity oscillation between values 1 and $\hat{k}(h)$, which depends on the inhomogeneity. Notice that $\hat{k}(0) = k$.

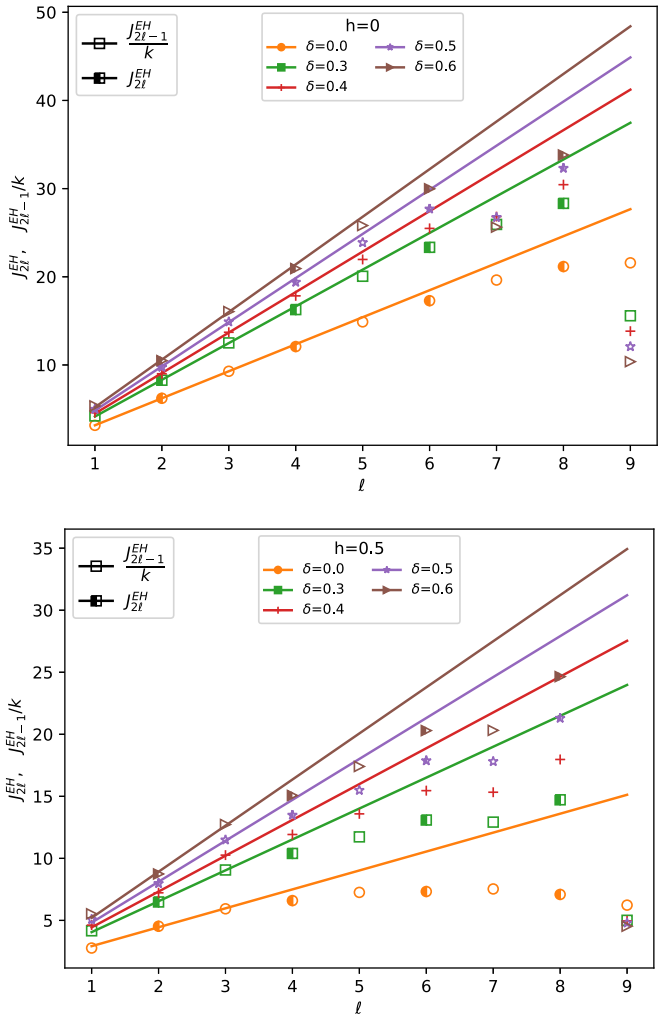

FIG. 10. Nearest-neighbor couplings of a chain of $2N = 20$ Majorana fermions, J_ℓ^{EH}, with a parity compensation: odd values of ℓ are divided by k. (a) Case $h = 0$. We can see that, despite the small size of the chain, we recover the behavior of the infinite chain near the boundary for strong dimerizations. Empty symbols correspond to even couplings while the filled ones are for $J_{2\ell-1}^{EH}/k$, see Eq. 69. (b) In the case $h = 0.5$, we observe the same initial behavior for low values of ℓ.

IV. CONCLUSIONS AND FURTHER WORK

In this work, we have characterized the entanglement properties of an inhomogeneous transverse field Ising critical spin-1/2 chain for which both the couplings and external fields fall exponentially from the center with a rate h, which defines the rainbow ITF model. It can be analytically solved by mapping into a Majorana chain, which suggests to treat the couplings and the external fields on an equal footing. Applying the strong disorder renormalization method we find that the ground state can be expressed in terms of generalized singlet states which are displayed concentrically around the center, similarly to the rainbow state. The weak inhomogeneity regime can be characterized by taking the continuum limit and showing that the resulting field theory corresponds to a free massless Majorana fermion field on a curved space-time. Thus we are able to predict the behaviour of the entanglement entropy deforming appropriately the known CFT results for Minkowski space-time, which turns the characteristic logarithmic growth into a linear growth with the block size. Moreover, there is a smooth crossover between both regimes. The nearest-neighbor coefficients of the entanglement Hamiltonian present the standard linear growth as we move away from the internal boundary, in agreement with the Bisognano-Wichmann theorem, showing that the state can be interpreted as a thermofield double for large enough inhomogeneity.

Out of criticality, we introduce an alternating term whose strength δ competes with h, attempting to destroy the linear entanglement. Strong-disorder renormalization arguments show that for each value of $\kappa \equiv \delta/h$ we obtain a fixed number of concentric singlets around the center of the chain, also showing that the trivial and nontrivial Kitaev phases are obtained for positive and negative values of κ, although with a substantial deformation. The weak inhomogeneity regime with small δ is described by a massive Majorana field theory placed over the curved space-time that we found in the case of the critical model. We have computed the EE by defining an effective correlation length $\xi_E(\delta, L)$ which is deformed with the metric, see Eq. (61). Near the entangling point, the entanglement Hamiltonian presents a linear growth of the couplings with a parity oscillation that can be accounted for using CTM results for the infinite systems. The amplitude of the oscillation and the slope depends on the inhomogeneity parameter.

In previous work [39], we found a connection between the rainbow states and SPT phases by means of a folding transformation around the center of the chain. In particular, we found a correspondence between the antiferromagnetic Heisenberg spin chain and the Haldane phase and another one between the rainbow XX spin chain and the BDI phase belonging to the classification of topological insulators made by Altland and Zirnbauer [71]. It could be interesting to extend this approach to the models considered in this manuscript and, more generally, to address the entanglement characterization of inhomogeneous 2D systems. In addition, it could be relevant to consider an experimental realization of the rainbow state in terms of a Rydberg atoms chain whose effective Hamiltonian is an inhomogeneous ITF model with an additional longitudinal field [72]. It is possible to extend Fisher's RG to this model and find the conditions under which a rainbow is formed. Also, it could be interesting to consider strongly inhomogeneous anyon models and study them harnessing their relation with $SU(2)_k$ Chern-Simons theories [60,62].

ACKNOWLEDGMENTS

We thank Gene Kim and Erik Tonni for conversations. We acknowledge the Spanish government for financial support through grants PGC2018-095862-B-C21 (NSSB and GS), PGC2018-094763-B-I00 (SNS), PID2019-105182GB-I00 (JRL), QUITEMAD+ S2013/ICE-2801, SEV-2016-0597 of the "Centro de Excelencia Severo Ochoa" Programme and the CSIC Research Platform on Quantum Technologies PTI-001.

APPENDIX A: SDRG ON MAJORANA CHAINS

In this Appendix, we explain the SDRG scheme applied to an inhomogeneous chain of Majorana fermions. Let us consider a system of four Majorana fermions whose Hamiltonian is given by:

$$H = i(g_{ia}\gamma_i\gamma_a + g_{ib}\gamma_i\gamma_b + g_{ab}\gamma_a\gamma_b + g_{aj}\gamma_a\gamma_j + g_{bj}\gamma_b\gamma_j), \tag{A1}$$

with $\{\gamma_m, \gamma_n\} = 2\delta_{mn}$. Let us assume that g_{ab} is larger than the rest so we can use use perturbation theory to diagonalize (A1).

$$H_0 = ig_{ab}\gamma_a\gamma_b, \tag{A2}$$

$$H_I = i(g_{ia}\gamma_i\gamma_a + g_{ib}\gamma_i\gamma_b - g_{ja}\gamma_j\gamma_a - g_{jb}\gamma_j\gamma_b). \tag{A3}$$

Defining the Dirac fermion $b = \frac{1}{2}(\gamma_a + i\gamma_b)$, we have that $H_0 = 2g_{ab}(b^\dagger b - 1/2)$ whose spectrum is $\pm|g_{ab}|$ and eigenvectors $|0\rangle, |1\rangle$ such that $b|0\rangle = 0$. The H_I can be written as

$$\begin{aligned} H_I =& i\{[(g_{ia} - ig_{ib})\gamma_i - (g_{aj} - ig_{bj})\gamma_j]b \\ &+ [(g_{ia} + ig_{ib})\gamma_i - (g_{aj} + ig_{bj})\gamma_j]b^\dagger\}. \end{aligned} \tag{A4}$$

Note that we must extend the Hilbert space: $|0\rangle \to |0\rangle \otimes |\psi\rangle$ where $|\psi\rangle$ is an unknown state of the Majorana fermions γ_i, γ_j. In the same way, $|1\rangle \to |1\rangle \otimes |\varphi\rangle$. However we shall make an abuse of notation and write γ_i instead of $\langle\psi|\gamma_i|\varphi\rangle$. The first-order corrections are zero so we compute the second order:

$$\Delta E_0 = \frac{\langle 0|H_I|1\rangle\langle 1|H_I|0\rangle}{E_0 - E_1}. \tag{A5}$$

Using Eq. (A4), we find the same corrections for $g_{ab} > 0$ and $g_{ab} < 0$

$$\Delta E_0 = i\left(\frac{g_{ia}g_{bj}}{g_{ab}} - \frac{g_{ib}g_{aj}}{g_{ab}}\right)\gamma_i\gamma_j + \tilde{E}, \tag{A6}$$

with $\tilde{E}_0 = 1/(2|g_{ab}|)(g_{ia}^2 + g_{ib}^2 + g_{bj}^2 + g_{aj}^2)$. Thus an effective Hamiltonian $H_{eff} = ig_{ij}\gamma_i\gamma_j$ emerge with the hopping term given by

$$g_{ij} = \frac{g_{ia}g_{bj}}{g_{ab}} - \frac{g_{ib}g_{aj}}{g_{ab}}. \tag{A7}$$

Particularizing for the ITF spin chain, $g_{ib} = g_{aj} = 0$ and we recover Eqs. (6) and (7). In Ref. [62], the authors provide the same result with a graphical derivation. The matrix elements are computed by counting the loops obtained by overlaying the (generalized) singlet states. See Appendix F for details of the overlaying procedure.

APPENDIX B: COVARIANCE MATRICES

Let us consider a system of $N = 2L$ Majorana fermions given by the quadratic Hamiltonian:

$$\mathcal{H} = i\boldsymbol{\gamma}^T A\boldsymbol{\gamma}, \tag{B1}$$

where $\boldsymbol{\gamma}^T = (\gamma_1 \dots \gamma_N)$ and $A = -A^T$. There exists a transformation $Q \in SO(2N)$ which brings the Hamiltonian to the canonical form

$$Q^T A Q = N_\epsilon, \tag{B2}$$

where N_ϵ is a block diagonal matrix

$$N_\epsilon = \left(\begin{array}{c|c} 0 & \boldsymbol{\epsilon} \\ \hline -\boldsymbol{\epsilon} & 0 \end{array}\right), \tag{B3}$$

where $\boldsymbol{\epsilon}$ is an $L \times L$ matrix with $\mathrm{diag}(\boldsymbol{\epsilon}) = (\epsilon_1, \dots, \epsilon_L)$, which are the positive eigenvalues of the matrix iA. We have then that

$$\mathcal{H} = i\boldsymbol{\gamma}^T A\boldsymbol{\gamma} = i\boldsymbol{\gamma}^T Q N_\epsilon Q^T\boldsymbol{\gamma} = i\tilde{\boldsymbol{\gamma}}^T N_\epsilon\tilde{\boldsymbol{\gamma}}, \tag{B4}$$

where we have defined a set of Majorana fermions $\tilde{\boldsymbol{\gamma}} = Q^T\boldsymbol{\gamma}$. These Majorana fermions can be arranged into Dirac fermions $\boldsymbol{\Psi}^T = (\boldsymbol{b}, \boldsymbol{b}^\dagger) = (b_1 \dots b_L, b_1^\dagger \dots b_L^\dagger)$ with $\boldsymbol{\Psi} = U\tilde{\boldsymbol{\gamma}}$ and

$$U = \left(\begin{array}{c|c} \mathbb{I} & i\mathbb{I} \\ \hline \mathbb{I} & -i\mathbb{I} \end{array}\right), \tag{B5}$$

where $\mathbb{I}$ is the $L \times L$ identity matrix. The Hamiltonian takes the form $\mathcal{H} = \sum_k \epsilon_k(b_k^\dagger b_k - 1)$ and the correlators are particularly simple,

$$\langle\boldsymbol{\Psi}\boldsymbol{\Psi}^\dagger\rangle = \left(\begin{array}{c|c} \mathbb{I} & 0 \\ \hline 0 & 0 \end{array}\right). \tag{B6}$$

We can express it back in terms of the Majorana fermions $\langle\boldsymbol{\Psi}\boldsymbol{\Psi}^\dagger\rangle = U\langle\tilde{\boldsymbol{\gamma}}\tilde{\boldsymbol{\gamma}}^T\rangle U^\dagger$ and those in terms of the physical Majorana fermions $\boldsymbol{\gamma}$,

$$\langle\boldsymbol{\gamma}\boldsymbol{\gamma}^T\rangle = Q^T\left(\begin{array}{c|c} \mathbb{I} & i\mathbb{I} \\ \hline -i\mathbb{I} & \mathbb{I} \end{array}\right)Q. \tag{B7}$$

The symmetric part of the matrix above is given by the anticommutation relation of the Majorana fermions, while the antisymmetric part that contains all the nontrivial information is known as the covariance matrix.

APPENDIX C: DIRAC FERMION IN CURVED SPACE-TIME

Let us consider the Dirac equation in curved space-time:

$$(i\not{D} - m)\Psi = 0, \tag{C1}$$

where $\not{D} = E_a^\mu\gamma^a D_\mu$ is the slashed covariant derivative, and $E_a^\mu = g^{\mu\nu}\eta_{ab}e_\nu^b$ is the inverse of the vielbein basis, actually a *zweibein*, e_μ^a that satisfies $g_{\mu\nu} = e_\mu^a e_\nu^b\eta_{ab}$. More precisely, the covariant derivative of the two component spinor Ψ is given by

$$D_\mu\Psi = \left(\partial_\mu - \frac{1}{8}\omega_\mu^{ab}[\gamma_a, \gamma_b]\right)\Psi, \tag{C2}$$

where ω_μ^{ab} is the spin-connection which is defined in terms of the Christoffel symbols $\Gamma_{\sigma\mu}^\nu$ and the inverse of the zweibein E_a^μ,

$$\omega_\mu^{ab} = e_\nu^a\partial_\mu E^{b\nu} + e_\nu^a E^{b\sigma}\Gamma_{\sigma\mu}^\nu, \tag{C3}$$

As we are considering a static system, it is reasonable to assume that the zweibein matrix e_μ^a is diagonal ($E_0^1 = E_1^0 = 0$). Expanding (C1) with this assumption leads to

$$\begin{aligned} &\left(iE_0^0\gamma^0\left(\partial_0 - \frac{1}{8}\omega_0^{ab}[\gamma_a, \gamma_b]\right)\right. \\ &\left. + iE_1^1\gamma^1\left(\partial_1 - \frac{1}{8}\omega_0^{ab}[\gamma_a, \gamma_b]\right) - m\right)\Psi = 0. \end{aligned} \tag{C4}$$

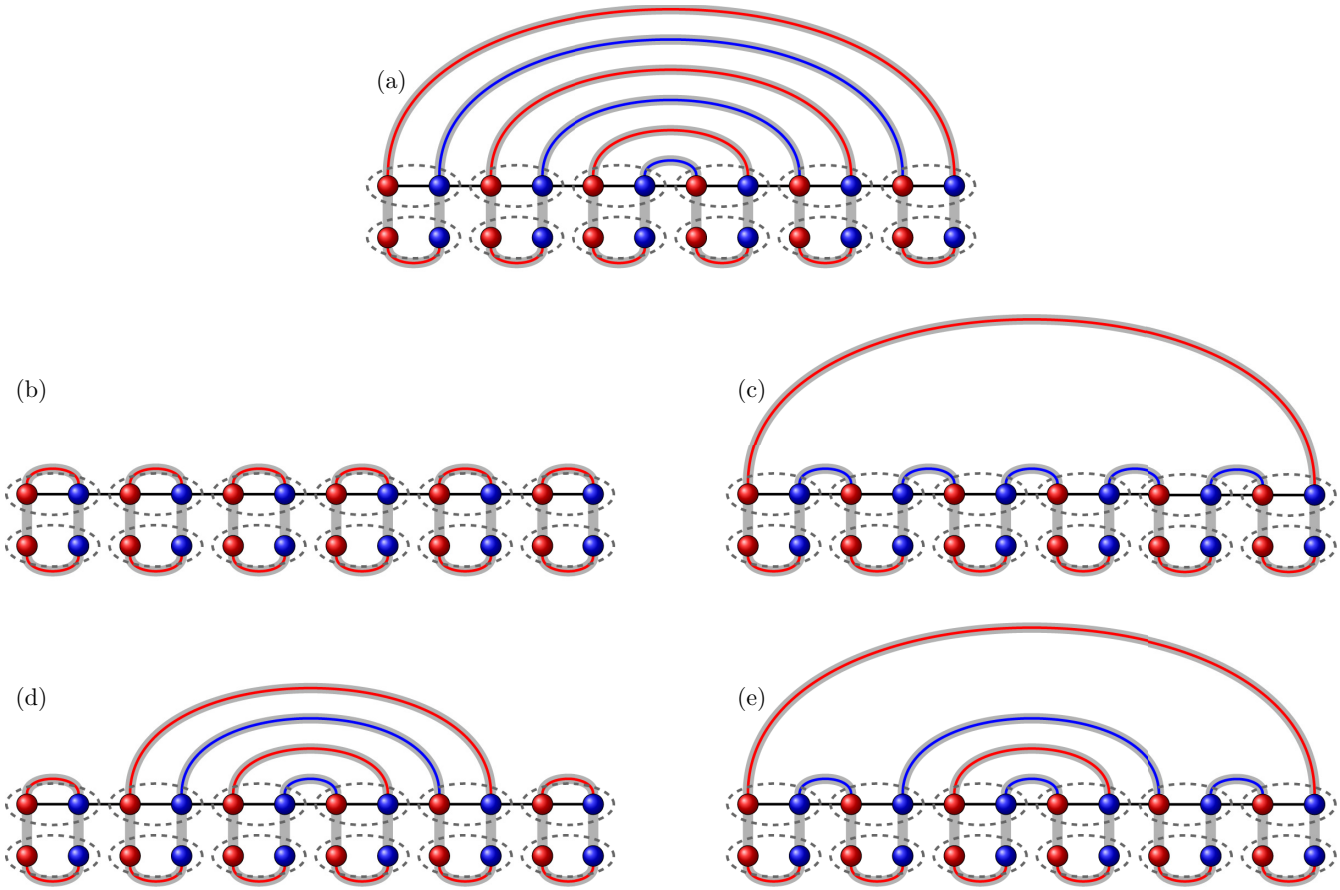

FIG. 11. Overlapping of the same states considered in Fig. 5. Discussion on the main text.

Taking into account that $[\gamma_0, \gamma_1] = [-\gamma^0, \gamma^1] = -2\gamma^3$ and the antisymmetry of the internal indices of the spin connection we arrive at

$$\left(\gamma^0\partial_0+\frac{1}{2}\omega_0^{01}\gamma^0\gamma^3+\frac{E_1^1}{E_0^0}\left(\gamma^1\partial_1+\frac{1}{2}\omega_1^{01}\gamma^1\gamma^3\right)+i\frac{m}{E_0^0}\right)\Psi=0. \tag{C5}$$

APPENDIX D: NONUNIVERSAL FUNCTION OF THE EE

The relation between the entanglement entropies of the XX and ITF models is given by [67]:

$$S_{\mathrm{XX}}(2x, 2L) = 2S_{\mathrm{ITF}}(x, L). \tag{D1}$$

We will compute the nonuniversal part of the EE (36) with the above expression. The EE of the XX model whose ground state is a RS has been studied in the past [36],

$$\begin{aligned}
S_{XX}(2x, 2L) &= S_{cft}(2x, 2L) + \frac{\gamma_1}{2} + S_{oscl}(2x, 2L),\\
S_{cft}(2x, 2L) &= \frac{1}{6}\ln\left[e^{-h|2x|}\frac{8(e^{h2L}-1)}{h\pi}\cos\left(\frac{\pi(e^{h|2x|}-1)}{2(e^{h2L}-1)}\right)\right],\\
S_{oscl}(2x, 2L) &= (-1)^{2x+2L}\\
&\quad\times\left[\frac{8(e^{h2L}-1)}{h\pi}\cos\left(\frac{\pi(e^{h|2x|}-1)}{2(e^{h2L}-1)}\right)\right]^{-1},
\end{aligned} \tag{D2}$$

and $\gamma_1 \approx 0.4950 + 1/3\ln 2$ [73]. Hence, by using relation Eq. (D1) we have

$$\begin{aligned}
c_I'(x, L) &= \frac{\gamma_1}{4} + \frac{1}{6}\ln 2\\
&\quad+(-1)^L\left[\frac{16(e^{2hL}-1)}{h\pi}\cos\left(\frac{\pi(e^{2h|x|}-1)}{4(e^{2hL}-1)}\right)\right]^{-1}.
\end{aligned} \tag{D3}$$

APPENDIX E: COMPUTATION OF THE ENTANGLEMENT HAMILTONIAN

The entanglement Hamiltonian can be obtained by knowing the covariance matrix. Consider a system of $N = 2L$ Majorana fermions given by the quadratic Hamiltonian (B1). There exists a transformation $O \in SO(2N)$ which brings the Hamiltonian to the canonical form $O^T A O = N_\epsilon'$, where N_ϵ' is a block diagonal matrix

$$N_\epsilon' = \bigoplus_k^L \begin{pmatrix} 0 & \epsilon_k \\ -\epsilon_k & 0 \end{pmatrix}, \tag{E1}$$

where $\pm\epsilon_k$, $k = 1, \ldots, L$ are the eigenvalues of the matrix iA. Notice that N_ϵ', Eq. (E1), and N_ϵ, Eq. (B3), are similar matrices meaning that O and Q differ in the order of the elements of the basis. The transformation O is more convenient because the lateral blocks considered in the main text are contiguous in this basis. Thus the Hamiltonian reads also as Eq. (B4) after

substituting Q by O. The density matrix ρ associated with the the GS of a quadratic Hamiltonian can always be written as

$$\rho = \mathcal{K} e^{-\mathcal{H}}, \tag{E2}$$

where $\mathcal{K}$ is a normalization constant and $\mathcal{H}$ is called the entanglement Hamiltonian (EH), given by (B1). It is possible to obtain $\mathcal{H}_A$, the EH associated to the reduced density matrix ρ_A by knowing the associated partial covariance matrix $\mathcal{C}_A = \langle \gamma_i \gamma_j \rangle$ with $i, j \in A$.

$$\mathcal{C}_A = O^T N'_\lambda O, \tag{E3}$$

N'_λ has the same structure as N'_ϵ but contains the eigenvalues of $\mathcal{C}_A$. Since the matrix O brings to the normal form both $\mathcal{C}_A$ and $\mathcal{H}_A$, there is a relation between the eigenvalues of the EH ϵ, known as entanglement spectrum (ES), and the eigenvalues of the covariance matrix:

$$\lambda_k = -\tanh \frac{\epsilon_k}{2} \tag{E4}$$

Hence, by inverting the above relation, it is possible to compute the EH knowing the covariance matrix,

$$\mathcal{H} = O^T N'_{\epsilon(\lambda)} O. \tag{E5}$$

APPENDIX F: PICTORIAL DISTINCTION OF THE TOPOLOGICAL PHASES

The trivial and topological ground states $|n\rangle$ of Eq. (4) can be distinguished graphically. We start by overlapping the GS with the trivial Majorana singlet state $\langle n|n=0\rangle$ and connecting the Majorana fermions (red and blue balls) with their opposites, leading to the formation of closed loops.

In Fig. 11, we show the same GS that we presented in Fig. 5 overlapping with $|n=0\rangle$, which we will call $\langle n=0|n=0\rangle$, that leads to N loops matching with the N Dirac fermions of kind c, see Eq. (3). This can be seen in panel (b). On the other side, the overlapping $\langle n=1|n=0\rangle$ leads to just one big loop as it can be seen in panel (c). Thus the topological phase is characterized by a big loop that encloses all the Majorana fermions. Considering $1 < n < L-2$ central decimations, the overlapping $\langle n=2m|n=0\rangle$ with $m=0,\ldots,L-1$ decreases the total number of loops to $N-m$ while the overlapping $\langle n=2m-1|n=0\rangle$ with $m=1,\ldots,L-1$ increases them up to m. For instance, in Fig. 11(d), we see the overlapping $\langle n=4|n=0\rangle$ that leads to $6-2=4$ bonds. In panel (e), there are 2 loops, because the overlapping corresponds to $\langle n=3|n=0\rangle$. Finally, as it can be seen in panel (a), the overlaying of a rainbow state $|\mathrm{RS}\rangle$ $n=0$ leads to $N/2$ loops. This is another way of unveiling the criticality of the RS since it corresponds to the intermediate situation.

The loops can also be interpreted in terms of spins and Fisher's RG [62]. Each loop contains those spins that were hybridized in consecutive RG steps with dominant J. Hence, the state $|n=1\rangle$ is a *superspin* while the RS can be seen as a collection of hybridized pairs of spins. However, notice that they do not form a SU(2) singlets as it occurs with the Dasgupta-Ma method applied to antiferromagnetic spin 1/2 chains.

[1] L. Amico, R. Fazio, A. Osterloh, and V. Vedral, Entanglement in many-body systems, Rev. Mod. Phys. **80**, 517 (2008).

[2] P. Calabrese, J. Cardy, and B. Doyon, Entanglement entropy in extended quantum systems, J. Phys. A: Math. Theor. **42**, 500301 (2009).

[3] N. Laflorencie, Quantum entanglement in condensed matter systems, Phys. Rep. **646**, 1 (2016).

[4] S. S. Roy, S. N. Santalla, J. Rodríguez-Laguna, and G. Sierra, Entanglement as geometry and flow, Phys. Rev. B **101**, 195134 (2020).

[5] B. Zeng, X. Chen, D. L. Zhou, and X. G. Wen, *Quantum Information Meets Quantum Matter* (Springer, New York, 2019).

[6] M. Srednicki, Entropy and Area, Phys. Rev. Lett. **71**, 666 (1993).

[7] M. B. Hastings, Solving gapped Hamiltonians locally, Phys. Rev. B **73**, 085115 (2006).

[8] M. M. Wolf, F. Verstraete, M. B. Hastings, and J. I. Cirac, Area Laws in Quantum Systems: Mutual Information and Correlations, Phys. Rev. Lett. **100**, 070502 (2008).

[9] J. Eisert, M. Cramer, and M. B. Plenio, Area-laws for the entanglement entropy: A review, Rev. Mod. Phys. **82**, 277 (2010).

[10] C. Holzhey, F. Larsen, and F. Wilczek, Geometric and renormalized entropy in conformal field theory, Nucl. Phys. B **424**, 443 (1994).

[11] G. Vidal, J. I. Latorre, E. Rico, and A. Kitaev, Entanglement in Quantum Critical Phenomena, Phys. Rev. Lett. **90**, 227902 (2003).

[12] P. Calabrese and J. Cardy, Entanglement entropy and quantum field theory, J. Stat. Mech.: Theory Exp. (2004) P06002.

[13] P. Calabrese and J. Cardy, Entanglement entropy and conformal field theory, J. Phys. A **42**, 504005 (2009).

[14] G. Refael and J. E. Moore, Entanglement Entropy of Random Quantum Critical Points in One Dimension, Phys. Rev. Lett. **93**, 260602 (2004).

[15] G. Refael and J. E. Moore, Criticality and entanglement in random quantum systems, J. Phys. A **42**, 504010 (2009).

[16] N. Laflorencie, Scaling of entanglement entropy in the random singlet phase, Phys. Rev. B **72**, 140408(R) (2005).

[17] M. Fagotti, P. Calabrese, and J. E. Moore, Entanglement spectrum of random-singlet quantum critical points, Phys. Rev. B **83**, 045110 (2011).

[18] G. Ramírez, J. Rodríguez-Laguna, and G. Sierra, Entanglement in low-energy states of the random coupling model, J. Stat. Mech.: Theory Exp. (2014) P07003.

[19] P. Ruggiero, V. Alba, and P. Calabrese, The entanglement negativity in random spin chains, Phys. Rev. B **94**, 035152 (2016).

[20] M. Campostrini and E. Vicari, Quantum critical behavior and trap-size scaling of trapped bosons in a one-dimensional optical lattice, Phys. Rev. A **81**, 063614 (2010).

[21] J. Dubail, J. M. Stephan, J. Viti, and P. Calabrese, Conformal field theory for inhomogeneous one-dimensional quantum systems: The example of non-interacting Fermi gases SciPost Phys. **2**, 002 (2017).

[22] S. Murciano, P. Ruggiero, and P. Calabrese, Entanglement and relative entropies for low-lying excited states in inhomogeneous one-dimensional quantum systems, J. Stat. Mech. (2019) 034001.

[23] H. Ueda and T. Nishino, Hyperbolic deformation on quantum lattice Hamiltonians, J. Phys. Soc. Jpn. **78**, 014001 (2009).

[24] S. Sachdev and J. Ye, Gapless Spin-Fluid Ground State in a Random Quantum Heisenberg Magnet, Phys. Rev. Lett. **70**, 3339 (1993).

[25] V. Rosenhaus, An introduction to the SYK model, J. Phys. A: Math. Theor. **52**, 323001 (2019).

[26] O. Boada, A. Celi, J. I. Latorre, and M. Lewenstein, Dirac equation for cold atoms in artificial curved spacetimes, New J. Phys. **13**, 035002 (2011).

[27] J. Rodríguez-Laguna, L. Tarruell, M. Lewenstein, and A. Celi, Synthetic Unruh effect in cold atoms, Phys. Rev. A **95**, 013627 (2017).

[28] B. Mula, S. N. Santalla, and J. Rodríguez-Laguna, Casimir forces on deformed fermionic chains, Phys. Rev. Res. **3**, 013062 (2021).

[29] F. Finkel and A. González-López, Inhomogeneous XX spin chains and quasi-exactly solvable models, J. Stat. Mech. (2020) 093105.

[30] C. Dasgupta and S.-K. Ma, Low-temperature properties of the random Heisenberg antiferromagnetic chain, Phys. Rev. B **22**, 1305 (1980).

[31] G. Vitagliano, A. Riera, and J. I. Latorre, Volume-law scaling for the entanglement entropy in spin 1/2 chains, New J. Phys. **12**, 113049 (2010).

[32] G. Ramírez, J. Rodríguez-Laguna, and G. Sierra, From conformal to volume-law for the entanglement entropy in exponentially deformed critical spin 1/2 chains, J. Stat. Mech. (2014) P10004.

[33] B. Alkurtass, L. Banchi, and S. Bose, Optimal Quench for Distance-Independent Entanglement andMaximal Block Entropy, Phys. Rev. A **90**, 042304 (2014).

[34] G. Ramírez, J. Rodríguez-Laguna, and G. Sierra, Entanglement over the rainbow, J. Stat. Mech. (2015) P06002.

[35] J. Rodríguez-Laguna, S. N. Santalla, and G. Ramírez, G. Sierra, Entanglement in correlated random spin chains, RNA folding and kinetic roughening, New J. Phys. **18**, 073025 (2016).

[36] J. Rodríguez-Laguna, J. Dubaîl, G. Ramírez, P. Calabrese, and G. Sierra, More on the rainbow chain: entanglement, spacetime geometry and thermal states, J. Phys. A **50**, 164001 (2017).

[37] E. Tonni, J. Rodríguez-Laguna, and G. Sierra, Entanglement hamiltonian and entanglement contour in inhomogeneous 1D critical systems, J. Stat. Mech. (2018) 043105.

[38] I. MacCormack, A. L. Liu, M. Nozaki, and S. Ryu, Holographic Duals of Inhomogeneous Systems: The Rainbow Chain and the Sine-Square Deformation Model, J. Phys. A: Math. Theor. **52**, 505401 (2019).

[39] N. S. Sáenz de Buruaga, S. N. Santalla, J. Rodríguez-Laguna, and G. Sierra, Symmetry protected phases in inhomogeneous spin chains, J. Stat. Mech.: Theory Exp. (2019) 093102.

[40] N. S. Sáenz de Buruaga, S. N. Santalla, J. Rodríguez-Laguna, and G. Sierra, Piercing the rainbow state: Entanglement on an inhomogeneous spin chain with a defect, Phys. Rev. B **101**, 205121 (2020).

[41] R. N. Alexander, A. Ahmadain, Z. Zhang, and I. Klich, Exact rainbow tensor networks for the colorful Motzkin and Fredkin spin chains, Phys. Rev. B **100**, 214430 (2019).

[42] V. Alba, S. N. Santalla, P. Ruggiero, J. Rodríguez-Laguna, P. Calabrese, and G. Sierra, Unsual area-law violation in random inhomogeneous systems, J. Stat. Mech.: Theory Exp. (2019) 023105.

[43] H. Li and F. D. M. Haldane, Entanglement Spectrum as a Generalization of Entanglement Entropy: Identification of Topological Order in Non-Abelian Fractional Quantum Hall Effect States, Phys. Rev. Lett. **101**, 010504 (2008).

[44] J. Bisognano and E. Wichmann, On the duality condition for a hermitian scalar field, J. Math. Phys. **16**, 985 (1975).

[45] J. Bisognano and E. Wichmann, On the duality condition for quantum fields, J. Math. Phys. **17**, 303 (1976).

[46] I. Peschel and V. Eisler, Reduced density matrices and entanglement entropy in free lattice models, J. Phys. A: Math. Theor. **42**, 504003 (2009).

[47] J. Cardy and E. Tonni, Entanglement Hamiltonians in two-dimensional conformal field theory, J. Stat. Mech. (2016) 123103.

[48] V. Eisler, E. Tonni, and I. Peschel, On the continuum limit of the entanglement Hamiltonian, J. Stat. Mech. (2019) 073101.

[49] V. Eisler, G. Di Giulio, E. Tonni, and I. Peschel, Entanglement Hamiltonians for non-critical quantum chains, J. Stat. Mech. (2020) 103102.

[50] A. Yu. Kitaev, Unpaired Majorana fermions in quantum wires, Phys.-Usp. **44**, 131 (2001).

[51] F. Pollmann, A. M. Turner, E. Berg, and M. Oshikawa, Entanglement spectrum of a topological phase in one dimension, Phys. Rev. B **81**, 064439 (2010).

[52] L Fidkowski and A. Kitaev, Topological phases of fermions in one dimension, Phys. Rev. B **83**, 075103 (2011).

[53] A. M. Turner, F. Pollmann, and E. Berg, Topological phases of one-dimensional fermions: An entanglement point of view, Phys. Rev. B **83**, 075102 (2011).

[54] X. Chen, Z. C. Gu, and X. G. Wen, Classification of Gapped Symmetric Phases in 1D Spin Systems, Phys. Rev. B **83**, 035107 (2011).

[55] F. Pollmann, E. Berg, A. M. Turner, and M. Oshikawa, Symmetry protection of topological order in one-dimensional quantum spin systems, Phys. Rev. B **85**, 075125 (2012).

[56] D. S. Fisher, Random antiferromagnetic quantum spin chains, Phys. Rev. B **50**, 3799 (1994).

[57] D. S. Fisher, Critical behavior of random transverse-field Ising spin chains, Phys. Rev. B **51**, 6411 (1995).

[58] V. Lahtinen and J. K. Pachos, A short introduction to topological quantum computation, SciPost Phys. **3**, 021 (2017).

[59] J. K. Pachos, *Introduction to Topological Quantum Computation* (Cambridge University Press, 2012).

[60] C. Nayak, S. H. Simon, A. Stern, M. Freedman, and S. Das Sarma, Non-Abelian anyons and topological quantum computation, Rev. Mod. Phys. **80**, 1083 (2008).

[61] C. Gomez, M. Ruiz-Altaba, and G. Sierra, *Quantum Groups in Two-Dimensional Physics*, Cambridge Monographs on Mathematical Physics (Cambridge University Press, Cambridge, 1996).

[62] N. E. Bonesteel and K. Yang, Infinite-Randomness Fixed Points for Chains of Non-Abelian Quasiparticles, Phys. Rev. Lett. **99**, 140405 (2007).

[63] L. Fidkowski, G. Refael, N. E. Bonesteel, and J. E. Moorec-theorem violation for effective central charge of infinite-randomness fixed points, Phys. Rev. B **78**, 224204 (2008).

[64] O. Motrunich, K. Damle, and D. A. Huse, Griffiths effects and quantum critical points in dirty superconductors without spin-rotation invariance: One-dimensional examples, Phys. Rev. B **63**, 224204 (2001).

[65] T. Devakul, S. N. Majumdar, and D. A. Huse, Probability distribution of the entanglement across a cut at an infinite-randomness fixed point, Phys. Rev. B **95**, 104204 (2017).

[66] I. Peschel, Calculation of reduced density matrices from correlation functions, J. Phys. A: Math. Gen. **36**, L205 (2003).

[67] F. Iglói and R. Juhász, Exact relationship between the entanglement entropies of XY and quantum Ising chains, Europhys. Lett. **81**, 57003 (2008).

[68] W. P. Su, J. R. Schrieffer, and A. J. Heeger, Solitons in Polyacetylene, Phys. Rev. Lett. **42**, 1698 (1979).

[69] A. Heeger, S. Kivelson, J. R. Schrieffer, and W.-P. Su, Solitons in conducting polymers, Rev. Mod. Phys. **60**, 781 (1988).

[70] M. Abramowitz and I. A. Stegun, *Handbook of Mathematical Functions with Formulas, Graphs, and Mathematical Tables* (US Government printing office, 1948), p. 590.

[71] A. Altland and M. R. Zirnbauer, Nonstandard symmetry classes in mesoscopic normal-superconducting hybrid structures, Phys. Rev. B **55**, 1142 (1997).

[72] P. Schauss, Quantum simulation of transverse Ising models with Rydberg atoms, Quantum Sci. Technol. **3**, 023001 (2018).

[73] B.-Q. Jin, V. E. Korepin, Quantum Spin Chain, Toeplitz Determinants and the Fisher–Hartwig conjecture, J. Stat. Phys. **116**, 79 (2004).